Journal of Nuclear Materials 385 (2009) 582–590

Contents lists available at ScienceDirect

Journal of Nuclear Materials

journal homepage: www.elsevier.com/locate/jnucmat

Fabrication of mesoporous and high specific surface area lanthanum carbide–carbon nanotube composites

L. Biasetto [a,b,*], S. Carturan [a], G. Maggioni [a], P. Zanonato [c], P. Di Bernardo [c], P. Colombo [b,d], A. Andrighetto [a], G. Prete [a]

[a] INFN-Laboratori Nazionali di Legnaro, V.le dell'Università 2, 35020 Legnaro (PD), Italy
[b] Università di Padova, Dipartimento di Ingegneria Meccanica, Via Marzolo 9, 35131 Padova, Italy
[c] Università di Padova, Dipartimento di Scienze Chimiche, Via Marzolo 1, 35131 Padova, Italy
[d] Department of Materials Science and Engineering, The Pennsylvania State University, University Park, PA 16802, USA

ARTICLE INFO

Article history:
Received 28 October 2008
Accepted 8 January 2009

ABSTRACT

Mesoporous lanthanum carbide–carbon nanotube composites were produced by means of carbothermal reaction of lanthanum oxide, graphite and multi-walled carbon nanotube mixtures under high vacuum. Residual gas analysis revealed the higher reactivity of lanthanum oxide towards carbon nanotubes compared to graphite. After sintering, the composites revealed a specific surface area increasing with the amount of carbon nanotubes introduced. The meso-porosity of carbon nanotubes was maintained after thermal treatment.

1. Introduction

ISOL (Isotope separator on line) facilities to produce radioactive ion beams are gaining significant interest world-wide because of the widespread possibilities they offer to extend our knowledge concerning the structure of the atomic nucleus, the formation of the stars, of the heavy-elements and the processes that govern the universe [1].

The SPES (Study for the Production of Exotic Species) project, now under development at LNL-INFN [2,3], is going to produce neutron rich isotopes ($Z > 40$) by directly impinging a 40 MeV proton beam of $I = 200$ μA, on uranium dicarbide porous thin disks (~1 mm). By this route, the facility should be able to produce 10^{13} fissions/s. However, the number of isotopes capable of being captured by the ionization source is a function of various parameters such as sticking time, half life, cross section, diffusion and effusion time [4].

In order to extract the highest possible number of isotopes, it is necessary to optimize parameters such as the target limiting temperature [5], its composition, microstructure, and permeability.

For all the above-mentioned reasons, the research on the optimization of the target properties is currently very lively [6–8]. Besides the parameters mentioned earlier, other important characteristics include the capability of working under vacuum (10^{-4} Pa) at temperature as high as 2000 °C for a reasonable time (some weeks), the crystalline grain size and porosity (amount, average size, shape and interconnectivity of the pores). For this reason, some attempts have been performed in order to produce low density, highly permeable targets [6,7].

The best candidate material possessing a good balance between all the above requirements has been demonstrated to be UC_x (that is, UC_2 dispersed in an excess of graphite) [5,9,10], typically obtained by carbothermal reduction of an appropriate oxide precursor or by the direct reaction between the metal and carbon. However, because of the difficulties related to safely handling the radioactive materials obtained with uranium, lanthanum have been proposed as substitute material for preliminary studies and investigations [7,11].

The discoveries of fullerenes and carbon nanotubes (CNTs) [12,13] as new structures in the nanoscale range have opened a challenging new field in solid state physics, chemistry and materials science with a wide spectra of possible applications. The prospect of heterostructures made from CNTs is of particular interest for nanodevices because of their useful size scale and their unique electronic properties. The possibility to combine nanotubes with metal carbides possessing properties suitable for interconnects in ultra-large-scale integrate circuits has been investigated in the last 10 years. The main difficulty in such devices is related to the control and purity of the nanojunction between the nanotubes and the metal carbide. Zhang et al. [14] report on a method based on a controlled solid–solid reaction: C (nanotubes) + M (solid) → MC (solid) to be performed in ultra-high vacuum or in an inert atmosphere to avoid any volatile reactants. Since the reaction is spatially restricted by partial contact between the surface of the solid reactant (M) and CNTs, it can be easily controlled, and predictions may be performed on the basis of diffusion coefficient calculations.

* Corresponding author. Address: Università di Padova, Dipartimento di Ingegneria Meccanica, Via Marzolo 9, 35131 Padova, Italy.
E-mail address: lisa.biasetto@lnl.infn.it (L. Biasetto).

0022-3115/$ - see front matter © 2009 Elsevier B.V. All rights reserved.
doi:10.1016/j.jnucmat.2009.01.035

Moreover, CNTs have been tested to reinforce various ceramics, cermets, metals and alloys because they possess many unique mechanical and physical properties [15–18]. The two main difficulties in such applications are related to:

- The poor solubilisation of the pristine multi-walled carbon nanotubes (MWCNTs) and the consequent severe structure inhomogenities.
- The poor connectivity between CNTs and the ceramic matrix.

In Ref. [19], multi-walled carbon nanotubes were coated with tungsten carbide (WC) by reduction and carburization and then used for doping WC–10Co cemented carbide (tungsten carbide in 10 wt% cobalt). A small amount of WC coated nanotubes (0.4 wt%) introduced in the WC-10Co cemented carbide resulted in a 32.8% improvement of the Transverse Rupture Strength (TRS) and 1.2% of the fracture toughness. However, larger amounts of MWCNTs caused a decrease in all mechanical properties (TRS, fracture toughness and Vickers hardness). Yamamoto et al. [20], recently proposed a novel structure for carbon nanotubes reinforced alumina composites, by means of acid-treated MWCNTs in solution with aluminium hydroxide and further spark plasma sintering at 1500 °C under a pressure of 20 MPa. The addition of only the 0.9 vol.% of acid-treated MWCNTs to alumina results in 27% and 25% simultaneous increase in bending strength and fracture toughness, respectively. Moreover an abrupt increase of electrical conductivity was observed.

In the literature, lanthanum carbide can be found together with CNTs because lanthanide (or rare earth) ions possess optical and magnetic properties that are particularly interesting when they are situated in a confined geometry. It has been suggested that materials encapsulated into the hollow regions of nanotubes could cause a significant change to the physical properties of nanotubes [21–23]. Therefore, a number of attempts have been made to fill these nanotubes with metals or metallic compounds to produce ultrafine conductor or semiconductor wires or nanometer-size composites [24]. Ruoff et al. [25] and Liu and Cowley [24] have demonstrated the encapsulation of lanthanum in CNTs and carbon nanoparticles. Awasthi et al. [26] have reported on synthesis by d.c. arc evaporation of lanthanum carbide nanotubes starting from lanthanum metal and graphite in helium atmosphere.

In the present study, lanthanum dicarbide–MWCNTs composites were produced by means of carbothermal reduction of La_2O_3 under high vacuum, where both graphite powders and carbon nanotubes were used as carbon source. The main scope of this study was the production of highly porous (high specific surface area) materials with improved thermo-mechanical properties, to be employed in the production of radioactive ion beams. The introduction of meso-porosity (pores in the range 2–50 nm) and the consequent increase in the material specific surface area could facilitate the processes of isotopes diffusion and effusion and consequently improve the target release efficiency.

2. Experimental

Lanthanum dicarbide–CNTs composite were synthesized by means of the carbothermal reduction of lanthanum oxide, in the presence of excess carbon, according to reaction (1):

$$La_2O_3 + 11C \rightarrow 2LaC_2 + 4C + 3CO_{(g)} \quad (1)$$

Both graphite and MWCNTs were used as carbon source, where the excess of carbon was calculated in order to obtain a final material with a LaC_2/C molar ratio equal to 1/2. This choice was prompted by previous studies on release efficiency of UC_x target materials [5,9,10]. La_2O_3 and graphite (mesh size −325) powders were purchased from Sigma–Aldrich and used as received. MWCNTs with outer average diameter of 8–15 nm and lengths up to 50 μm were purchased from Guangzhou Heji Trade Co. (China), and used as received. Powders were manually mixed and grinded in an agatha mortar where a 2–4 wt% of phenolic resin in acetone solution at 10 wt% was added as binder. Powders were uniaxially pressed at 750 MPa and after extraction were heat treated under high vacuum (10^{-4} Pa) in a graphite furnace [27] up to 1500 °C, following the heat treatment schedule reported in Table 1.

The heat treatment was designed on the basis of the results of mass spectrometry analysis. The desorption of gaseous products while continuously heating up to 1600 °C (heating rate 0.5 °C/min) the LC and L100CNT samples (refer to Table 2) in two separate runs was monitored by a quadrupole mass spectrometer (Prisma Plus QMG220 M3, Pfeiffer Vacuum Inc., USA), connected to the graphite furnace. The evolution of CO, CO_2 and H_2O was monitored following the 28, 44 and 18 m/e peaks.

Sample compositions were designed in order to assess the effect of the amount of MWCNTs on selected properties of the final material. In Table 2, an overview of the samples prepared is reported.

The labelling in Table 2 is referred to the weight amount of MWCNTs introduced, compared to the total amount of carbon corresponding to Eq. (1). After carburization and sintering, samples were immediately transferred to an inert atmosphere glove box (H_2O and O_2 < 1 ppm) in order to prevent the reaction between lanthanum dicarbide and humid air.

A rough estimation of the amount of porosity (p) of the prepared samples was calculated following Eq. (2):

$$p = 1 - \rho_b/\rho_t \quad (2)$$

where the bulk density was measured as $\rho_b = m_{tot}/V_{tot}$ The theoretical true density (ρ_t in Eq. (2)) was calculated taking into account the stoichiometric ratios for LaC_2 and C in Eq. (1), as the weighted average of the densities of bulk LaC_2 (5.02 g/cm^3, Espimetals MSDS) graphite (1.90 g/cm^3, Aldrich MSDS) and MWCNTs, assuming the true density of MWCNTs the same as graphite.

The morphology and composition of the prepared samples were investigated by means of a Scanning Electron Microscope (Philips XL-30, SEM) equipped with Energy Dispersive Spectrometer (EDS) probe. Crystalline phases of the samples were studied by means of an X-ray diffractometer (Philips PW 1710, XRD) in Bragg–Brentano configuration using a Cu Kα radiation. Powders were protected from the environment by means of a 25 μm PEEK® film (kindly supplied by Victrex Europa GmbH, Hofheim, Germany).

Specific surface area (SSA) and Pore Size Distribution (PSD) of treated bulk samples and as received MWCNTs were obtained from nitrogen adsorption–desorption measurements at 77 K using an ASAP 2020 (Micromeritics Italia Srl, Milano, Italy) instrument.

Table 1
Heat treatment schedule.

Heating rate	1st plateau	2nd plateau	Cooling rate
2 °C/min	1250 °C, 12 h	1500 °C, 24 h	2 °C/min

Table 2
Overview of the prepared samples.

Sample label	La_2O_3 (wt%)	Graphite (wt%)	MWCNTs (wt%)
LC	71.2	28.8	–
LC25CNT	71.2	21.6	7.2
LC50CNT	71.2	14.4	14.4
LC75CNT	71.2	7.2	21.6
L100CNT	71.2	–	28.8

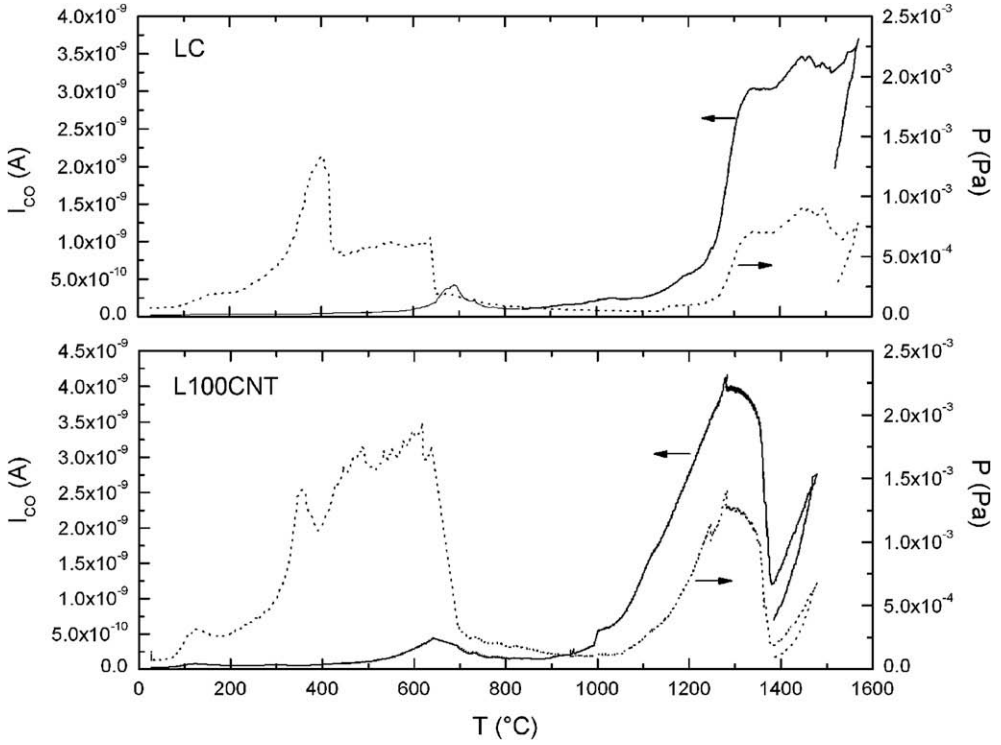

Fig. 1. The pressure (Pa) and CO ion current (A) for samples LC (top) and L100CNT (bottom).

The samples were previously degassed under vacuum (0.3 Pa) at 300 °C for at least 15 h prior to sorption analysis. The nitrogen adsorption data were collected in the relative pressure range (P/P_0) of $10^{-2} < P/P_0 < 1$ where P_0 is defined as the vapor pressure of the adsorbing gas (nitrogen) at the temperature at which the test is conducted (77 K). To obtain an accurate characterization of the microporous region (according to IUPAC notation, micropores have diameter of less than 2 nm, mesopores have pore diameter between 2 nm and 50 nm and macropores have pore diameter greater than 50 nm), a sufficient number of data points in the low pressures regime is needed, which requires the addition of constant small nitrogen volumes. Hence, successive nitrogen doses of 5 cm^3/g were added until $P/P_0 = 0.01$ was reached. Subsequently, further nitrogen was added and the gas volumes required to obtain a fixed set of relative pressures, up to a value of 1.00, were measured. Specific surface areas (SSAs) were calculated from N_2 adsorption data at relative pressures below 0.20, by the multipoint Brunauer–Emmett–Teller (BET) method [28,29]. Data were also analyzed by the *t-plot* method [30] and by the Barrett–Joyner–Halenda (BJH) method [31], using the manufacturer's software. The micropores size distribution was calculated using the Hovarth–Kawazoe analysis for cylindrical pore geometry [32].

3. Results and discussion

The mass spectrometer analysis revealed that in the first stage of the heat treatment decomposition of the phenolic resin, used as binder, generates mainly water and a minority amount of CO.

In Fig. 1 the CO evolution is plotted against temperature for both LC and L100CNT samples.

Two are the main differences between La_2O_3/CNTs and La_2O_3 /graphite systems:

1. The carburization of La_2O_3 powders starts at lower temperature when the carbon source is the MWCNTs.
2. The reaction involving the CNTs graphene layers is complete at 1350 °C, that involving graphite (sample LC) starts at 1250 °C and takes place gradually up to 1500 °C.

The shoulder at the end of the LC carburization process and present also in the L100CNT at approximately 1600 °C is due to the furnace out-gassing, as confirmed by a blank run.

This first thermal treatment guided the design of the following experiments as depicted in Table 1.

Samples LC25CNT, LC50CNT and LC75CNT were treated in one batch; in Fig. 2, the pressure upon carburization and sintering plotted against temperature is shown. Three distinct regions can

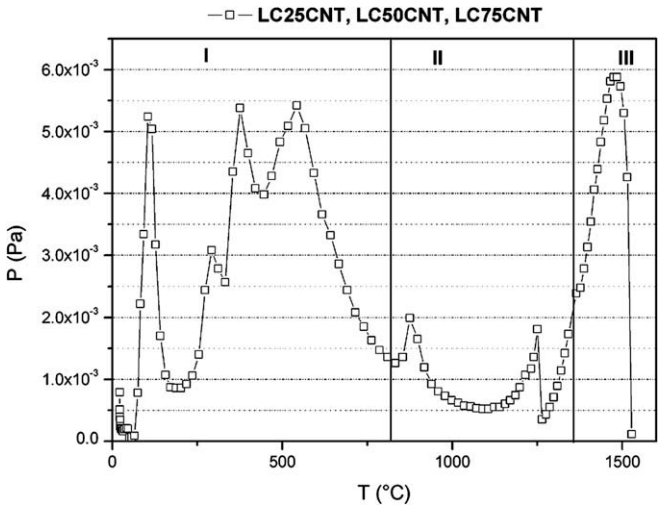

Fig. 2. The pressure (Pa) plotted against the temperature (°C) during the heat treatment for samples LC25CNT, LC50CNT, LC75CNT.

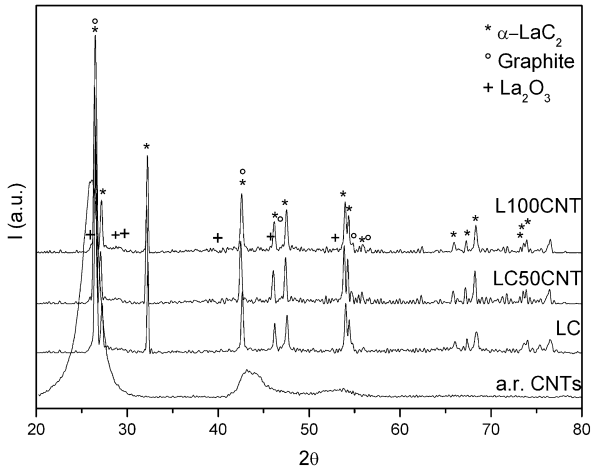

Fig. 3. XRD for CNTs (as received) and for samples LC, LC50CNT, and L100CNT.

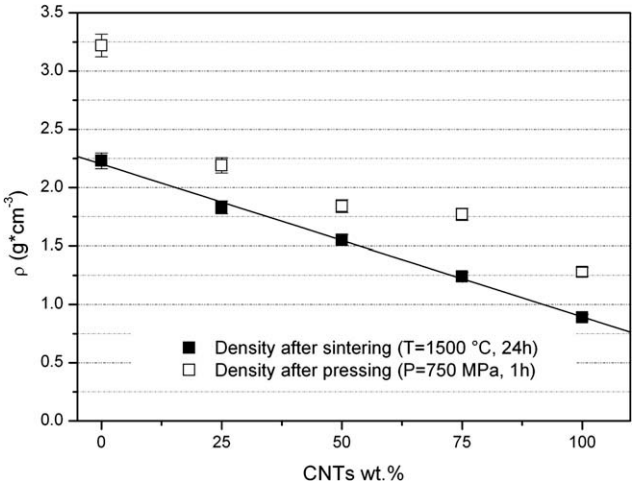

Fig. 4. Bulk density variation before and after thermal treatment, as a function of the amount of CNTs.

be observed. The first region (I, maximum temperature 900 °C) corresponds to the sample out-gassing and phenolic resin decomposition. The second region (II) can be associated to the carburization that occurs at temperatures ranging from 1100 °C to 1500 °C; the pressure starts to rise at 1100 °C and increases up to 1250 °C, where a pressure decrease is recorded due to the 12 h plateau at this temperature (see also Table 1). Indeed, the 12 h dwell time is not sufficient to complete the reaction as graphite reacts at higher temperature than CNTs; in fact, the pressure increases once the temperature starts to increase towards the final sintering temperature. However, this increase in pressure may also partially be attributed to the experimental set-up out-gassing as observed in Fig. 1. The region III can be associated to the sample sintering, where the carbothermal reaction is complete and the pressure consequently decreases.

After carburization and sintering, the samples could be easily handled without breaking, even in the case of that containing the highest CNTs weight percentage. The XRD analysis revealed that in all samples (even in L100CNT) the signals due to La_2O_3 are absent and consequently the carburization process can be considered complete with formation of tetragonal LaC_2 (see Fig. 3).

Weight losses measured for the samples after carburization/sintering also revealed that the reaction according to Eq. (1) was complete (Table 3). The estimated weight decrease due to carbothermal reaction, is 18.3 wt%; however, in samples containing CNTs, a higher weight loss is recorded. This can be at least in part attributed to the higher amount of binder (4 wt% instead of 2 wt% for LC) that was introduced in the starting mixture, and to the difficulty to remove the solvent of the binder from the green pellets containing CNTs. Moreover the pristine nanotubes generally possess some weight amount of impurities that could have been removed by the thermal treatment.

Fig. 4 shows that in the green samples containing CNTs, the density decreases as the CNTs amount increases. Moreover, also in the sintered samples, the bulk density linearly decreases as the wt% of the CNTs' increases, varying from 2.23 g/cc for the sample containing no CNTs (LC) to 0.89 g/cc for L100CNT. This is a well known behavior of composites containing CNTs due to their rope-like structure. Moreover, Fig. 4 shows that the density variation from the green samples to the sintered samples is much more significant for sample LC than for samples containing CNTs. The sample volumes measured before and after thermal treatment revealed that the LC sample shrinks approximately 5–10%, the samples containing CNTs present reduced shrinkage and the sample L100CNT shows an inverse behavior, expanding its volume by 10% after thermal treatment.

Nitrogen adsorption/desorption isotherms for the as-received carbon nanotubes (CNTs) are reported in Fig. 5, whereas the isotherms for the lanthanum carbide/CNTs systems containing different amounts of CNTs are compared in Fig. 6.

The pure CNTs sample exhibits moderate N_2 uptake at very low relative pressures, typical of partially microporous materials, whereas very low uptake is observed for the lanthanum carbide

Table 3
Measured values for weight loss and calculated total porosity (see also Eq. (2) in the experimental part).

Sample	Δwt%	*p*%
LC	19	24.2
LC25CNT	23.5	48.6
LC50CNT	23.5	57
LC75CNT	23.7	58.8
L100CNT	23.5	70.3

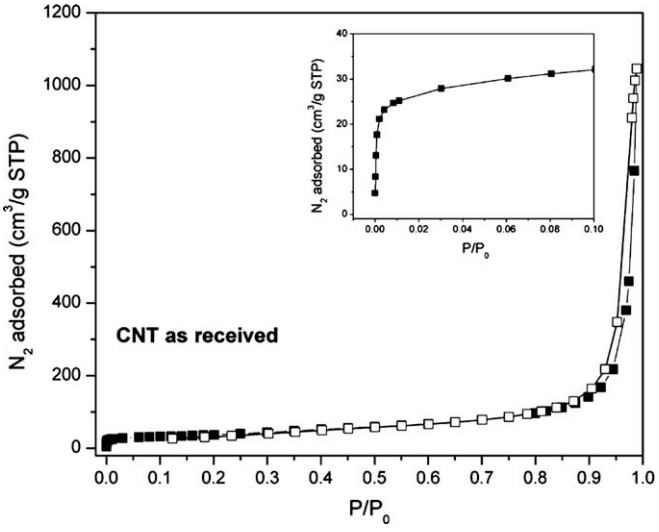

Fig. 5. Adsorption–desorption isotherms of N_2 (77 K) for the as received carbon nanotubes (closed symbol: adsorption, open symbol: desorption). The inset graph is an enlarged view of the low pressures region, where the steep rise induced by the presence of micropores can be appreciated.

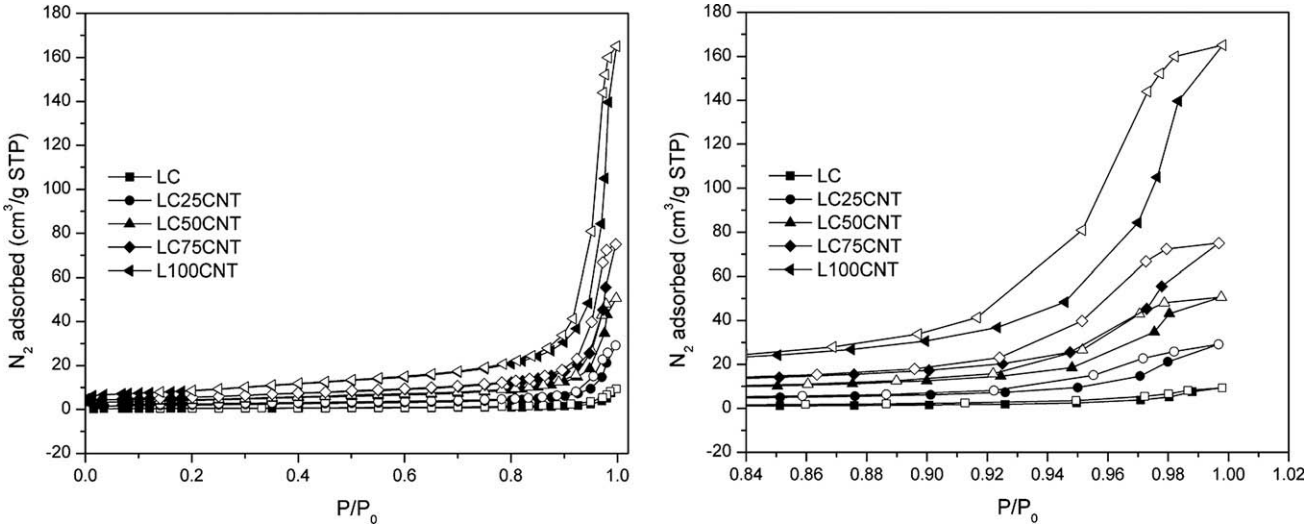

Fig. 6. Adsorption–desorption isotherms of N_2 (77 K) for the samples containing different amounts of CNTs (closed symbol: adsorption, open symbol: desorption). On the right side, the region at high pressures is enlarged.

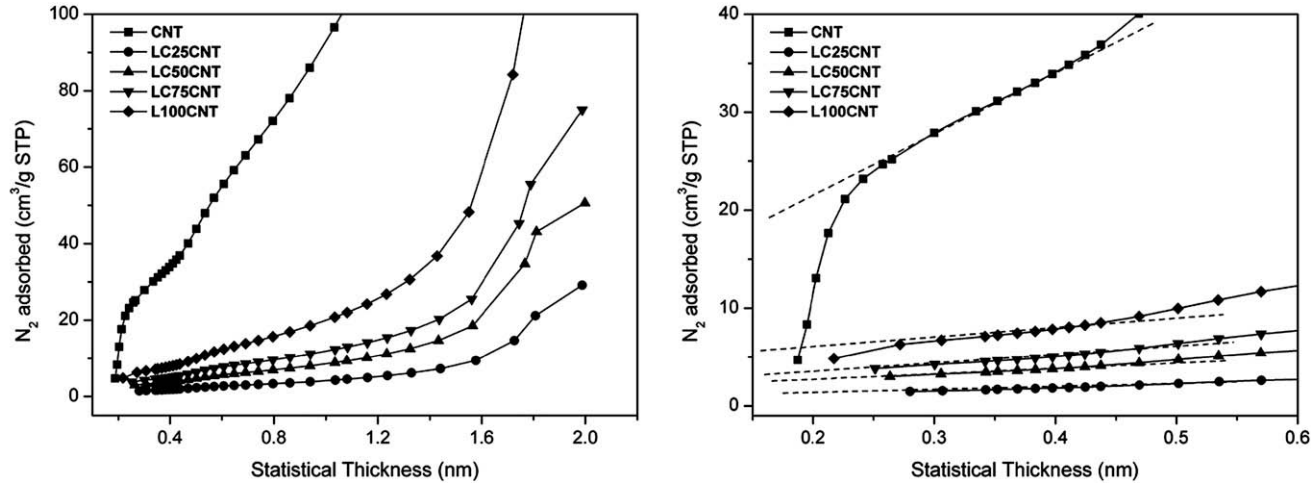

Fig. 7. *t-Plots* for the bare CNTs and the samples containing different amounts of CNTs. On the right side the enlarged view of the region corresponding to low P/P_0 values is reported. The dashed lines show the linear extrapolations used for the estimation of micropore volume.

based systems. On the other hand, at higher relative pressures the pure CNTs sample and the lanthanum carbide samples containing CNTs display significant similarities, as for the shape of isotherm curve (a type IV isotherm, according to the notation of Brunauer [33], which indicates the presence of mesopores) and for the presence of the hysteresis loop (the desorption curve lies above the adsorption curve), which closes in the high relative pressure region. The sample without CNTs displays negligible nitrogen adsorption, thereby proving to be non porous in the micro–meso-porosity range. The isotherms trends therefore suggest that samples containing CNTs are essentially mesoporous, while carbon nanotubes possess some micro-porosity in addition to meso-porosity. However, the fixed amount of 5 cm^3/g dosed onto samples below $P/P_0 = 0.01$ was indeed too high for the detailed characterization of micro-porosity for CNTs containing samples; for this reason, as it will be discussed in detail below, the Horwath–Kavazoe model applied to derive the micropore size distribution does not allow the accurate determination of the pore size. As for the determination of the micropore volume, the *t-plot* method [30] allows assessment of external surface area and micropore volume by plotting the adsorbed volume against the statistical thickness t of the adsorbed nitrogen layer. The method is based upon the fact that the total adsorption results from the sum of the adsorption in the micropores and on the external surface. It uses a thickness curve type Harkins and Jura [34], in a relative pressure range between 0.05 and 0.7 to compare the experimental results with the standard isotherm expected for N_2 adsorption on a non-porous solid [29]. An isotherm identical to the standard would have a *t-plot* straight line passing through the origin.

Fig. 7 shows the *t-plots* (amount adsorbed against the statistical thickness of the N_2 film) for the different samples analyzed. For all the samples, meso-porosity gives rise to an upward deviation of the *t-plot* in the high-pressure region, while micro-porosity distorts the *t-plot* in the low-pressure region. In Table 4 the principal features of the samples, obtained by the analysis of physisorption measurements, are reported. Analysis of the *t-plot* (using the Harkins–Jura thickness equation) [34] for the pure carbon nanotubes gives a micropore volume of 0.012 cm^3/g and a micropore surface area of 26.7 m^2/g (Table 4) which, compared to the total specific surface area of CNTs (130 m^2/g), suggests that not much more than 20% of the total surface area is associated with micropores. Similarly, the micropore volume and the micropore surface area values

Table 4
Surface area and characteristics of the porosity of mesoporous composite materials based on LaC_2 and CNTs.

Sample label	SSA (m^2/g)[a]	Micropore surface area (m^2/g)[b]	Total pore volume (cm^3/g)[c]	Micropore volume (t-plot) (cm^3/g)	Mesopores size (BJH) (nm)	Micropores size (HK) (nm)
CNTs	130.0	26.7	1.182	0.012	2.4, 52	1.2
LC	1.6	n.a.	0.008	n.a.	n.a.	n.a.
LC25CNT	7.0	1.3	0.033	0.0006	2.6, 45	n.a.
LC50CNT	14.4	3.6	0.066	0.0015	2.7, 49	n.a.
LC75CNT	19.3	4.1	0.086	0.0018	2.7, 43	n.a.
L100CNT	29.8	7.1	0.216	0.0031	2.7, 44	n.a.

[a] Specific surface area from the BET equation in the range of relative pressure $0.06 < P/P_0 < 0.2$.
[b] From the linear extrapolation of the *t-plot* in the range of statistical thickness 0.35–0.45 nm.
[c] Specific total pore volume at $P/P_0 \sim 0.98$ (adsorption branch).

for the samples containing CNTs and lanthanum carbide indicate that most of the specific surface area is associated with mesopores and that the fraction of micropores is about 20%.

The meso-porosity of the samples was further characterized by BJH analysis of the desorption curves, which indicated a bimodal distribution of pore sizes with a maximum at around 45–50 nm for all the samples and a small fraction of mesopores with size of about 2.5 nm (Fig. 8).

Micropore size distributions (PSD) were obtained using the Hovarth–Kawazoe (HK) approach [32], with the cylindrical-pore geometry proposed by Saito and Foley [35]. The pore models used are, obviously, simplistic and the absolute numbers should be treated with caution. In the case of pure CNTs, HK analysis indicates that the sample has an appreciable concentration of pores of 1.2 nm size, as shown in Fig. 9, whereas the lanthanum carbide samples containing CNTs do not display a reliable PSD curve, owing to the limited number of experimental data acquired in the low pressure range, as previously explained.

The presence of micropores with diameter of about 1.2 nm in the CNTs is most likely associated with small apertures between the walls of the CNTs formed when they twist together tightly. The presence of such micropores was already evidenced in previous studies concerning MWCNTs [36]. Due to the large outer diameter of the CNTs (8–15 nm from factory data sheet), the apertures are not likely to be very small because of geometric constraints, and these results reflect the almost complete absence of micropores smaller than 1.2 nm. The PSD of the pure CNTs and of the LC

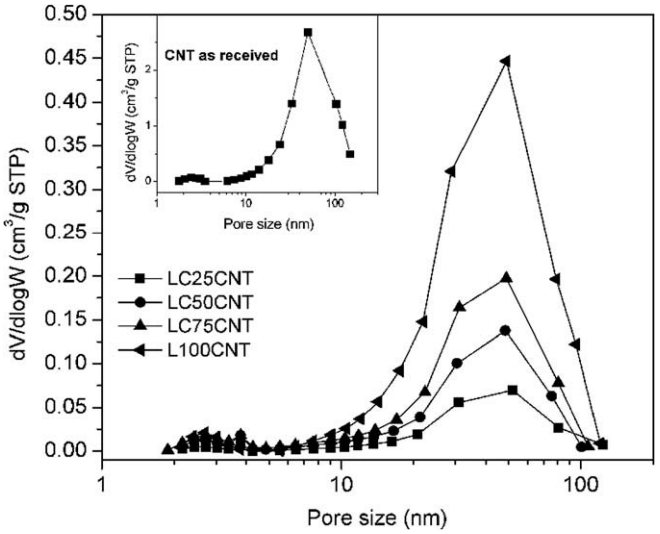

Fig. 8. BJH differential mesopore volume distributions for pure CNTs and samples containing CNTs in different amounts. For the sake of clarity, the curve for pure CNTs is reported in the inset graph.

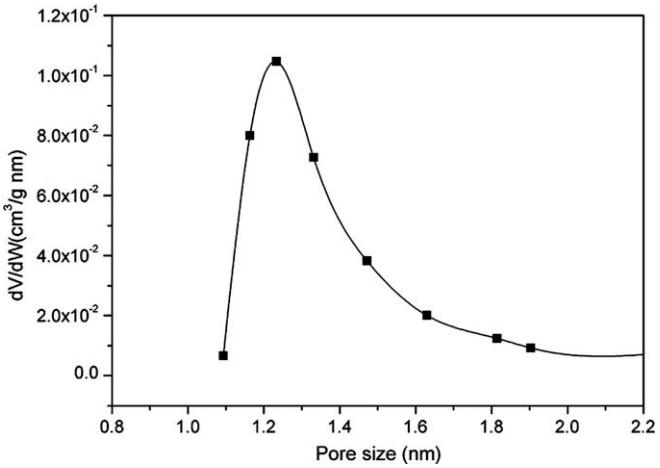

Fig. 9. Hovarth–Kawazoe differential pore volume plot–cylinder pore geometry (Saito/Foley) for pure CNTs.

samples also show a maximum at 2.4–2.7 nm in the mesoporous region (Fig. 8). Taking into account that the outer diameter of the CNTs is 8–15 nm this peak, according to the model proposed by Smajda and co-workers [37], can be assigned to the mesopores formed between two MWCNTs touching each other in sections where they either run parallel or cross each other, whereas the peak at 45–50 nm can be related to the slits between bundles of CNTs.

The results of this study point out that the introduction of carbon nanotubes in the starting mixtures greatly affects the specific surface area and the micro–meso-porosity of the final lanthanum carbide sintered samples. The graph in Fig. 10 demonstrates an almost linear correlation between the amount of CNTs introduced in the starting mixture and the specific surface area derived from BET analysis of the adsorption isotherms. In addition, this study shows that the fraction of micropore volume over the total pore volume is about 20% both in the pure CNTs and in the LC series and the mesopores size distribution from BJH are very similar with a bimodal distribution of pores centered at around 2.5 and 50 nm.

The morphology of the samples obtained according to the procedure described in Section 2 was examined by means of SEM. Fig. 11 shows the top surface of the samples, observed at the same magnification.

Three different parts can be distinguished in the SEM images, the dark and dense graphite grains (labelled as 1), the light grey lanthanum carbide sintered grains (labelled as 2) and the dark grey filamentous mass comprised of carbon nanotubes bundles (labelled as 3). The presence of such CNTs bundles reveals that nanotubes were not uniformly dispersed in the mixture, thus

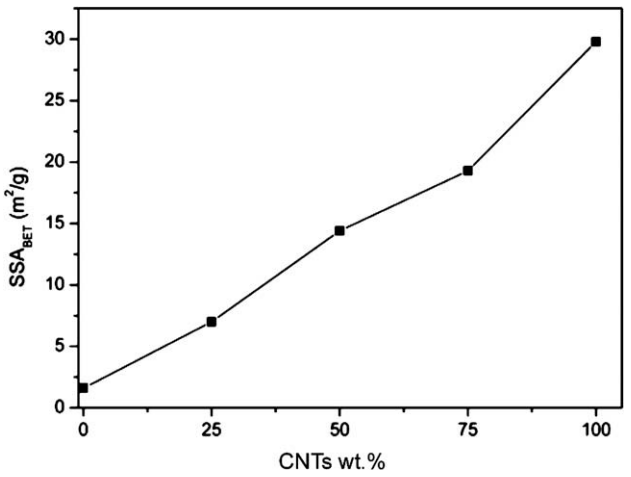

Fig. 10. Plot of the specific surface area of the samples containing CNTs vs. the amount of CNTs.

suggesting that for future experiments, more sophisticated dispersions techniques [19,20] should be used to achieve better homogeneity. In all samples, the high degree of sintering achieved by lanthanum carbide can be observed. The formation of lanthanum carbide is confirmed also in the sample without graphite in the starting mixture, where the only carbon source for the carbothermal reduction reaction comes from carbon nanotubes. A closer inspection of the sample L100CNT, shown in Fig. 12, reveals that lanthanum carbide grains are similar in shape and size to those found in the sample LC, without carbon nanotubes. The entanglement of MWCNTs as a result of their long length and high surface energy is also highlighted in the photo at high magnification reported in Fig. 12. The grain size of the sintered lanthanum carbide grains ranges from a few microns to 10 μm, and the grain morphology is anisotropic. Several macro-voids are also visible in the samples, with size ranging from a few μm up to 10–20 μm, thereby confirming that a fraction of macropores is also present, in addition to micro–mesopores, in agreement with previous work [8]. EDS spectra, also reported in Fig. 12, were collected from the different regions for the samples LC and L100CNT, which constitute the extremes of the present experiment from a compositional point of view, the former being without CNTs and the latter being without graphite. The atomic composition detected by focussing the beam spot on the light grey grains, using the same analytical conditions for both the samples (beam spot size and beam energy) indicates the presence of C, O and La, thus proving that the grains are composed of lanthanum carbide, in agreement with the XRD results reported in Fig. 3, with a thin layer of lanthanum hydroxide, resulting from sample exposure to humidity, as previously reported [7].

The EDS spectrum relative to the nanotubes in the sample L100CNT reveals the presence of La, besides C and traces of O. It can be proposed that at temperatures higher than 1100 °C the reactant lanthanum oxide interacts with the surface graphitic layers of MWCNTs forming in situ lanthanum carbide coated nanotubes. The reaction proceeds through the nucleation and growth of lanthanum carbide crystals which separate from the CNTs bundle and undergo aggregation and sintering as the temperature reaches 1500 °C. Since the amount of MWCNTs used in these experiments largely exceeds the stoichiometric ratio required for the formation of LaC_2 only, it can be proposed that the CNTs bundles still visible in the SEM images represent the stoichiometric excess and that the presence of lanthanum on the nanotubes

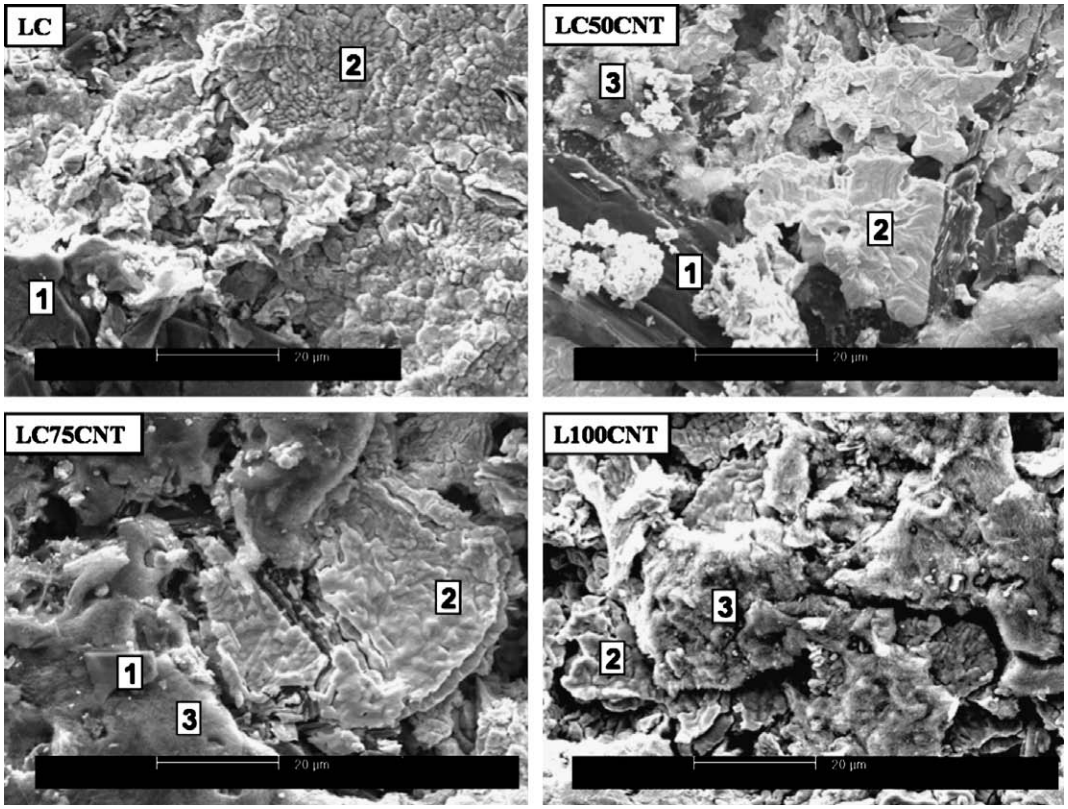

Fig. 11. SEM micrographs of the samples containing different amounts of CNTs, taken at the same magnification (label 1 graphite grains, label 2 LaC_2 grains, label 3 CNTs bundles).

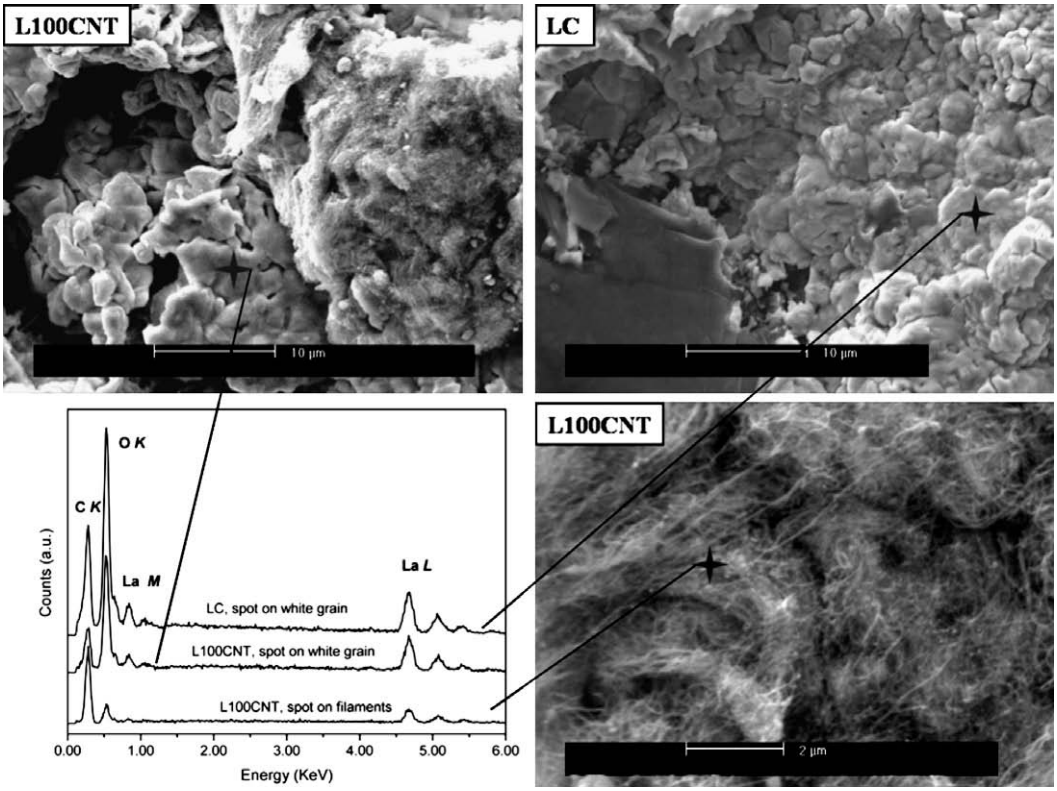

Fig. 12. SEM micrographs at high magnification of sample L100CNT (without graphite) and sample LC (without CNTs). The EDS spectra collected from lanthanum carbide grains and CNTs are reported for comparison.

surface provides a confirmation for the proposed mechanism of lanthanum carbide grain formation. It can be considered also that the surface diffusion along the length of the CNTs is much faster than bulk diffusion and consequently a different reaction rate may occur between the surface and the bulk of CNTs. Further experiments are currently under development and samples from starting mixtures of lanthanum oxide and MWCNTs in stoichiometric amounts will be produced in order to obtain a better knowledge of these systems.

4. Conclusions

LaC_2–MWCNTs composites are produced by means of direct carbothermal reaction of La_2O_3, MWCNTs and graphite mixtures. The effects of the introduction of CNTs in the starting mixtures are:

1. The diffusive solid state reaction between La_2O_3 and MWCNTs used as the sole carbon source is complete at the same conditions adopted for the samples prepared using graphite as the carbon source (samples L100CNT and LC, respectively).
2. The bulk density of the samples decreases with increasing the amount of CNTs and the calculated total porosity consequently increases ranging from 24.2% of the total volume for sample LC to 70.3% for sample L100CNT.
3. The total porosity could be attributed to three different kinds of pores: micro and mesopores directly deriving from the MWCNTs and macropores deriving from the CO release of carbothermal reaction. In all the samples produced in this work mesopores with a bimodal pore size distribution ranging from 45–50 nm to <3 nm are measured. Specific surface area linearly increases with increasing the amount of MWCNTs ranging from 1.6 m^2/g for sample LC to 29.8 m^2/g for sample L100CNT.

Acknowledgment

Authors are grateful to Reinhard Veljovic from VICTREX Europa GmbH, Hofheim, Germany, for kindly supplying the 25 μm PEEK film.

References

[1] G.D. Alton, J.R. Beene, Y. Liu, Nucl. Instrum. and Meth. A 438 (1999) 190.
[2] A. Andrighetto, S. Cevolani, C. Petrovich, Eur. Phys. J. A 25 (2005) 41.
[3] A. Andrighetto, S. Cevolani, C. Petrovich, M. Santana, Eur. Phys. J. A 30 (2006) 591.
[4] M. Dombsky, P. Bricault, P. Schmor, M. Lane, Nucl. Instrum. and Meth. B 204 (2003) 191.
[5] Y. Zhang, G.D. Alton, Nucl. Instrum. and Meth. A 521 (2004) 72.
[6] Y. Kawai, G.D. Alton, J.C. Bilheux, Nucl. Instrum. and Meth. B 241 (2005) 991.
[7] S. Carturan, M. Tonezzer, L. Piga, P. Zanonato, P. Colombo, A. Andrighetto, L. Biasetto, P. DiBernardo, G. Maggioni, F. Gramegna, G. Prete, Nucl. Instrum. and Meth. A 583 (2007) 256.
[8] L. Biasetto, P. Zanonato, S. Carturan, P. DiBernardo, P. Colombo, A. Andrighetto, G. Prete, J. Nucl. Mater. 378 (2008) 180.
[9] H.L. Ravn, T. Bjornstad, P. Hoff, O.C. Jonsson, E. Kugler, S. Sundell, B. Vosicki, ISOLDE Collaboration, Nucl. Instrum. and Meth. B 26 (1987) 183.
[10] J.P. Greene, T. Burtseva, J. Neubauer, J.A. Nolen, A.C.C. Villari, I.C. Gomes, Nucl. Instrum. and Meth. B 241 (2005) 986.
[11] P. Bricault, M. Dombsky, J. Lassen, F. Ames, TRIUMF Internal PrePrint, TRI-PP-07-31, November 2007.
[12] H.W Kroto et al., Nature 318 (1985) 162.
[13] S. Iijima, Nature 354 (1991) 56.
[14] Y. Zhang, T. Ichihashi, E. Landree, F. Nihey, S. Iijima, Science 285 (1999) 1719.
[15] Z.J. Jia, Z.Y. Wang, C.L. Xu, J. Liang, B.Q. Wei, D.H. Wu, S.W. Zhu, Mater. Sci. Eng. A 271 (1999) 395.
[16] Y.Q. Liu, L. Gao, Carbon 43 (2005) 47.
[17] Z. Xia, L. Riester, W.A. Curtin, H. Li, B.W. Sheldon, J. Liang, B. Chang, J.M. Xu, Acta Mater. 52 (2004) 931.19.
[18] Y. Morisada, Y. Miyamoto, Mater. Sci. Eng. A 381 (2004) 57.
[19] X. Shi, H. Yang, S. Wang, G. Shao, X. Duan, Mater. Sci. Eng. A 486 (2008) 489.
[20] G. Yamamoto, M. Omori, T. Hashida, H. Kimura, Nanotechnology 19 (2008) 1.
[21] J.W. Mintmire, B.I. Dunlap, C.T. White, Phys. Rev. Lett. 68 (1992) 631.
[22] N. Hamada, S. Sawada, A. Oshiyama, Phys. Rev. Lett. 68 (1992) 1579.

[23] K. Laasonen, W. Andreoni, M. Parrinello, Science 258 (1992) 1916.
[24] M. Liu, M. Cowley, Carbon 33 (1995) 225.
[25] R.S. Ruoff, D.C. Lorents, B. Chan, R. Malhotra, S. Subramoney, Science 259 (1993) 346.
[26] K. Awasthi, A.K. Singh, O.N. Srivastava, J. Nanosci. Nanotech. 2 (2002) 67.
[27] L. Biasetto, M. Manzolaro, A. Andrighetto, Eur. Phys. J. A. 38 (2008) 167–171.
[28] S. Brunauer, P.H. Emmett, E. Teller, J. Am. Chem. Soc. 60 (1938) 309.
[29] S.J. Gregg, K.S.W. Sing, Adsorption, Surface Area and Porosity, Academic Press, London, 1982. p. 285.
[30] B.C. Lippens, B.G. Linsen, J.H. de Boer, J. Catal. 3 (1964) 32.
[31] E.P. Barret, L.G. Joyner, P.H. Halenda, J. Am. Chem. Soc. 53 (1951) 373.
[32] G. Hovarth, K. Kawazoe, J. Chem. Eng. Jpn. 16 (1983) 470.
[33] S. Brunauer, The Adsorption of Gases and Vapors, vol. I, Physical Adsorption, Princeton, 1945.
[34] W.D. Harkins, G. Jura, J. Am. Chem. Soc. 66 (1944) 1366.
[35] A. Saito, H. Foley, AIChE J. 37 (1991) 429.
[36] F. Li, Y. Wang, D. Wang, F. Wei, Carbon 42 (2004) 2375.
[37] R. Smajda, A. Kukovecz, Z. Konya, I. Kiricsi, Carbon 45 (2007) 1176.